Available online at www.sciencedirect.com
ScienceDirect
Carbohydrate Research 342 (2007) 2396–2403
Carbohydrate RESEARCH

Theoretical investigation of hydrogen bonding effects on oxygen, nitrogen, and hydrogen chemical shielding and electric field gradient tensors of chitosan/HI salt

Sajjad Khodaei,[a] Nasser L. Hadipour[a,*] and Mohammad Reza Kasaai[b]

[a]*Department of Chemistry, Tarbiat Modares University, PO Box 14115-175, Tehran, Iran*
[b]*Faculty of Agriculture, Mazandaran University, Khazar Abad Road, Km. 9, PO Box 578, Sari, Mazandaran, Iran*

Received 8 May 2007; received in revised form 4 July 2007; accepted 12 July 2007
Available online 24 July 2007

Abstract—A density functional theory study has been carried out to calculate the ^{17}O, ^{15}N, ^{13}C, and ^{1}H chemical shielding as well as ^{17}O, ^{14}N, and ^{2}H electric field gradient tensors of chitosan/HI type I salt. These calculations were performed using the B3LYP functional and 6-311++G (d,p) and 6-31++G (d,p) basis sets. Calculated EFG and chemical shielding tensors were used to evaluate the ^{17}O, ^{14}N, and ^{2}H nuclear quadruple resonance, NQR, and ^{17}O, ^{15}N, ^{13}C, and ^{1}H nuclear magnetic resonance, NMR, parameters in the cluster model, which are in good agreement with the available experimental data. The difference in the isotropic shielding (σ_{iso}) and quadrupole coupling constant (C_Q) between monomer and target molecule in the cluster was analyzed in detail. It was shown that both EFG and CS tensors are sensitive to hydrogen-bonding interactions, and calculating both tensors is an advantage. A different influence of various hydrogen bond types, N–H···I, O–H···I, and N–H···O was observed on the calculated CS and EFG tensors. On the basis of this study, nitrogen and O-6 are the most important nuclei to confirm crystalline structure of chitosan/HI. These nuclei have large change in their CS and EFG tensors because of forming intermolecular hydrogen bonds. Moreover, the quantum chemical calculations indicated that the intermolecular hydrogen-bonding interactions play an essential role in determining the relative orientation of CS and EFG tensors of O-6 and nitrogen atoms in the molecular frame axes.

Keywords: Chitosan; Chitosan/HI type I salt; ^{17}O, ^{15}N, ^{13}C, and ^{1}H Chemical shielding; ^{17}O, ^{14}N, and ^{2}H Electric field gradient tensor; Density functional theory; Euler angles

1. Introduction

Chitosan, poly[β-(1→4)-D-glucosamine], is one of the most abundant biopolymers that has recently become an interesting subject in many fields of science, as well as in industry because of its extensive applications, for example, in wastewater treatment, cosmetics, biomedicine, and biology among other areas.[1–7] Chitosan is a cationic polysaccharide produced by deacetylation of chitin, a substance derived from the exoskeleton of crustaceans. The amine and hydroxyl groups of this polymer can bind to heavy metal ions and organic/inorganic acids to yield complexes and salts, respectively, which have been extensively studied by various techniques including X-ray diffraction, electron diffraction, ^{13}C and ^{15}N NMR spectroscopy, and FTIR spectroscopy.[8–19]

Hydrogen bond (HB) interactions play an important role of forming the molecules and crystal structure conformations of solid polysaccharides; therefore, characterizing HB properties can reveal useful trends about their bio-physicochemical properties and applications.[20] X-ray diffraction is a prime tool to characterize HB properties; however, it is insufficient to locate the accurate positions of hydrogen atoms in the structures considered. Solid-state nuclear magnetic resonance (NMR) spectroscopy is a powerful technique to study various types of HB properties.[21,22] Since the characteristic nature of HB is electrostatic, electric field gradient

* Corresponding author. E-mail: hadipour@modares.ac.ir

0008-6215/$ - see front matter © 2007 Elsevier Ltd. All rights reserved.
doi:10.1016/j.carres.2007.07.014

(EFG) and chemical shielding (CS) tensors at the sites of quadrupole and magnetic nuclei, respectively, are very sensitive to HB effects in hydrogen-bonded systems. The EFG and CS tensors can either be calculated by quantum chemical calculations or measured experimentally in forms of quadrupole coupling constants, C_Q, and isotropic chemical shifts, δ_{iso}, respectively. Although experimental measurements are essential in the investigation of molecular structures, however, high-level quantum chemical calculations have a determining role in the interpretation of observable measurements.

In the present work a density functional theory study is carried out to calculate the solid-state NMR parameters in crystalline chitosan/HI type I salt obtained by a recent X-ray diffraction study of Lertworasirikul et al.[23] Chitosan/HI type I salt was chosen for the study because iodine is the heaviest halide, and this work should reveal representative trends for other hydrogen halide complexes of chitosan. As mentioned earlier, since the EFG and CS tensors are very sensitive to HB interactions, those possible interacting neighbor contributors to HB with the target molecule were considered in a hydrogen-bonded cluster in NMR and EFG calculations (see Fig. 1 and Table 1 for details). The calculated EFG tensors at the sites of ^{17}O, ^{14}N, and ^{2}H nuclei are presented in Tables 3–5 and the calculated CS tensors at the sites of ^{17}O, ^{15}N, ^{13}C, and ^{1}H nuclei are listed in Tables 2–5 for two model systems of Chitosan/HI type I salt, the monomer and the target molecule in a cluster.

It is well-known that NMR properties are quite sensitive to relativistic effects in systems containing heavy atoms. This contribution arises from heavy-atom core regions where the velocity of the electron is high. Considering previous works, DFT-based approaches can be used to theoretically calculate the major relativistic effects on the shielding of light nuclei, the spin–orbit coupling.[24,25] Vaara and co-workers indicated that at the BW91 level of theory, the DFT method gives smaller relativistic effects than multi-configuration SCF (MCSCF) in CX_2 (X = O, S, Se, Te) series of compounds.[26]

2. Computational methods

Two model systems of chitosan/HI type I salt were considered in NMR and EFG calculations using the GAUSSIAN 98[27] package. Model I is a hydrogen-bonded cluster of chitosan/HI type I salt consisting of those possible interacting neighbor contributors to HB, where the target molecule and model II is a non-hydrogen-bonded (monomer) form of the considered structure. Both models are created by X-ray coordinates (see Fig. 1 and Table 1 for details).[23] Since X-ray diffraction cannot locate the accurate positions of hydrogen atoms, the hydrogen atoms of the crystalline structure were optimized at the level of B3LYP/6-31++G (d,p), whereas the other atom positions remained frozen during the optimization. The EFG and CS tensor calculations were carried out at the level of B3LYP. The gauge-included atomic orbital (GIAO)[28] approach was used to calculate the CS tensors. The basis sets employed in the EFG and CS calculations are 6-311++G (d,p) and 6-31++G (d,p) while LANL2DZ basis set was for iodide ions.[29] Based on our pervious experiences, 6-311++G (d,p) and 6-31++G (d,p) usually lead to satisfactory EFG and CS values.[30–33] However, since the hydrogen-bonded cluster was too complex to be studied computationally, the local density (LD)[34,35] method was used to save calculation time. In the LD method, the target molecule and those neighboring nuclei that were directly contrib-

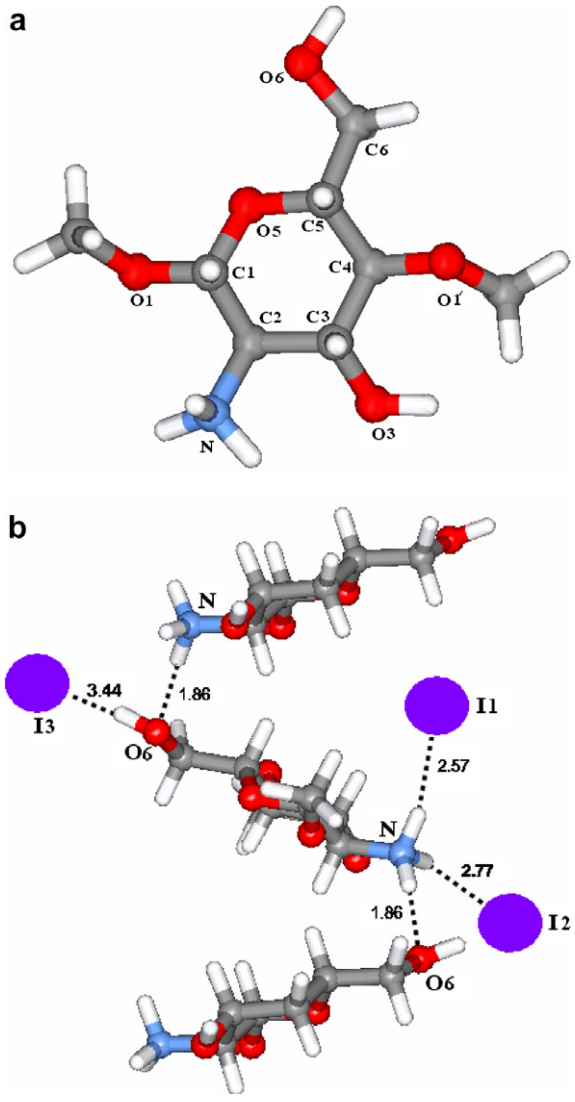

Figure 1. (a) Monomer, (b) illustration of the intermolecular HBs in the crystalline chitosan/HI salt.

Table 1. Details of HBs among chains and iodide ions in chitiosan/HI salt

Donor (D)	Acceptor (A)	$r_{(D\cdots A)}$ (Å)	$r_{(H\cdots A)}$ (Å)	∠(D–H···A) (degree)
N	I-1	3.52	2.57	154.85
O-6	I-2	3.44	2.50	162.4
N	I-3	3.70	2.77	150.31
N	O-6	2.84	1.86	157.62

uted to HB with the target molecule were calculated at the level of 6-311++G (d,p) and 6-31++G (d,p) basis sets; however, the other nuclei were calculated at the level of 6-31G and LANL2DZ basis sets. It is noted that the calculations for the monomeric form of chitosan/HI were also performed at the level of 6-311++G (d,p) and 6-31++G (d,p) basis sets.

Quantum chemical calculations yield the EFG tensors at the principal axis system (PAS) by assuming that $|q_{zz}| > |q_{yy}| > |q_{xx}|$. Experimentally, the quadrupole coupling constant, C_Q, which represents the interaction between electric quadrupole moment, eQ, and the EFG tensors at the sites of quadrupole nuclei, is measured (see Eq. 1). The standard Q values reported by Pyykkö[36] are used in Eq. 1: $Q(^{17}O) = -25.58$ mb,

Table 2. Calculated ^{13}C NMR parameters of cluster model[a,b]

Nuclei	σ_{11} (ppm)	σ_{22} (ppm)	σ_{33} (ppm)	σ_{iso} (ppm)	$\delta_{Cal.}$ (ppm)	$\delta_{Exp.}$ (ppm)	$\Delta_{(\delta_{Cal.}-\delta_{Exp.})}$
C-1	61.1	77.5	103.3	80.6	105.5	98.7	6.8
	[74.3]	[89.3]	[113.7]	[92.4]	[91.7]		[−7]
C-5	84	101.9	140.6	108.9	75.2	73.8	1.4
	[95.9]	[111.0]	[149.4]	[118.8]	[65.3]		[−8.5]
C-6	90.5	117	146	117.8	66.3	61.3	5
	[100.9]	[127.2]	[156.4]	[128.2]	[55.9]		[−5.4]
C-2	111.4	125.4	135.8	124.2	59.9	55.6	4.3
	[123.6]	[133.0]	[143.0]	[133.2]	[50.9]		[−4.7]
C-3	79.9	105	134.5	106.5	77.6	70	7.6
	[93.1]	[117.3]	[144.3]	[118.2]	[65.9]		[−4.1]
C-4	68.9	80.8	119.2	89.6	94.5	84.7	9.8
	[81.5]	[89.2]	[127.7]	[99.5]	[84.6]		[−0.1]

[a] Experimental values from Ref. 13.
[b] The values in brackets are calculated at the level of 6-31++G (d,p) and those out of brackets are calculated at the level of 6-311++G (d,p).

Table 3. Calculated oxygen NMR and NQR parameters[a]

Nuclei	Model	σ_{11} (ppm)	σ_{22} (ppm)	σ_{33} (ppm)	σ_{iso} (ppm)	$\delta_{Cal.}$ (ppm)	C_Q (MHz)	η_Q
O-1	Cluster	214.3	257.6	333.2	268.4	39.5	11.6	0.89
		[227.1]	[265.3]	[333.2]	[275.2]	[32.7]	[10.4]	[0.89]
	Monomer	197.5	249.8	319.8	255.7	52.2	11.7	0.85
		[215.0]	[260.8]	[332.5]	[269.5]	[38.4]	[10.7]	[0.86]
O-3	Cluster	234.4	254.2	272.8	253.8	54.1	11.5	0.97
		[247.9]	[267.1]	[281.5]	[265.5]	[42.4]	[10.4]	[0.98]
	Monomer	244.1	271.6	292.8	269.5	38.4	11.2	0.96
		[259.1]	[286.3]	[302.5]	[282.7]	[25.2]	[10.3]	[0.98]
O-5	Cluster	166.1	258.2	261.9	228.8	79.1	11.6	0.88
		[182.5]	[270.4]	[273.2]	[242.0]	[65.9]	[10.5]	[0.87]
	Monomer	157.1	211.2	244.3	204.2	103.7	12.1	0.87
		[175.8]	[225.8]	[259.8]	[220.4]	[87.5]	[11.0]	[0.86]
O-6	Cluster	200.6	283.5	318.3	267.5	40.4	9.45	0.91
		[184.2]	[269.7]	[317.2]	[257.0]	[50.8]	[8.51]	[0.92]
	Monomer	273.8	287.5	369.3	310.2	−2.32	12.0	0.82
		[259.7]	[275.2]	[364.9]	[299.9]	[7.97]	[11.1]	[0.80]

[a] The values in brackets are calculated at the level of 6-31++G (d,p), and those out of brackets are calculated at the level of 6-311++G (d,p).

Table 4. Calculated nitrogen NMR and NQR parameters

Basis sets	Model	σ_{11} (ppm)	σ_{22} (ppm)	σ_{33} (ppm)	σ_{iso} (ppm)	$\delta_{Cal.}$ (ppm)	$\delta_{Exp.}$[a] (ppm)	C_Q (MHz)	η_Q
6-31++G**	Cluster	189.6	208.5	211.2	203.1	20.28	—	−1.28	0.48
	Monomer	212.8	227.1	240.9	226.9	−3.53	~13	0.24	0.42
6-311++G**	Cluster	178.9	198.3	202.9	193.4	30.04	—	−1.46	0.48
	Monomer	196.2	212.4	226.7	211.8	11.65	~13	0.27	0.41

[a] From Ref. 14.

Table 5. Calculated hydrogen NMR and NQR parameters[a]

Nucleus	Model	σ_{11} (ppm)	σ_{22} (ppm)	σ_{33} (ppm)	σ_{iso} (ppm)	$\delta_{Cal.}$ (ppm)	C_Q (kHz)	η_Q
N–H···I-1	Cluster	9.17	13.8	44.9	22.6	9.07	214.9	0.05
		[9.27]	[14.0]	[44.7]	[22.7]	[9.04]	[204.1]	[0.05]
	Monomer	22.8	25.8	36.7	28.4	3.29	236.7	0.02
		[22.5]	[25.4]	[36.6]	[28.2]	[3.54]	[226.5]	[0.02]
N–H···I-2	Cluster	12.9	15.3	40.8	23.0	8.70	205.1	0.05
		[12.9]	[15.1]	[41.4]	[23.1]	[8.57]	[193.8]	[0.05]
	Monomer	18.3	26.0	35.6	26.6	5.07	219.9	0.02
		[17.9]	[25.6]	[35.5]	[26.4]	[5.34]	[209.6]	[0.02]
N–H···O-6	Cluster	13.9	19.0	42.0	25.0	6.72	208.3	0.07
		[13.9]	[19.1]	[42.0]	[25.0]	[6.70]	[198.2]	[0.07]
	Monomer	20.4	23.0	37.2	26.9	4.83	220.1	0.02
		[20.0]	[22.6]	[37.1]	[26.6]	[5.12]	[210.4]	[0.03]
O-6–H···I-3	Cluster	9.96	15.8	53.3	26.4	5.32	263.6	0.15
		[9.87]	[15.8]	[53.2]	[26.3]	[5.39]	[258.4]	[0.15]
	Monomer	21.1	27.6	44.1	31.0	0.74	295.5	0.15
		[20.4]	[27.0]	[44.0]	[30.5]	[1.21]	[288.8]	[0.16]

[a] The values in brackets are calculated at the level of 6-31++G (d,p), and those out of brackets are calculated at the level of 6-311++G (d,p).

$Q(^{14}N) = 20.44$ mb, and $Q(^{2}H) = 2.86$ mb. The other important parameter that can either be measured experimentally or calculated computationally is the asymmetry parameter, η_Q, meaning the deviation of EFG tensors from cylindrical symmetry (see Eq. 2). The converted EFG parameters for ^{17}O, ^{14}N, and ^{2}H nuclei are presented in Tables 3–5:

$$C_Q\ (\mathrm{MHz}) = e^2 Q q_{zz} h^{-1} \quad (1)$$

$$\eta_Q = |(q_{yy} - q_{xx})/q_{zz}| \quad (2)$$

The calculated CS tensors in PAS ($\sigma_{33} > \sigma_{22} > \sigma_{11}$) can also be converted to experimentally measurable isotropic chemical shift, δ_{iso}, by Eq. 3, where the isotropic CS can be calculated by Eq. 4. The values of $\sigma_{iso,ref}$ in Eq. 3 used for various nuclei are the following: $\sigma_{iso,ref}(^{17}O) = 307.9$ ppm,[37] $\sigma_{iso,ref}(^{15}N) = 223.4$ ppm,[38] $\sigma_{iso,ref}(^{13}C) = 184.1$ ppm,[39] $\sigma_{iso,ref}(^{1}H) = 31.69$ ppm. The calculated CS parameters for ^{17}O, ^{15}N, ^{13}C, and ^{1}H nuclei are listed in Tables 2–5:

$$\delta_{iso}\ (\mathrm{ppm}) = \sigma_{iso,ref} - \sigma_{iso} \quad (3)$$

$$\sigma_{iso}\ (\mathrm{ppm}) = (\sigma_{11} + \sigma_{22} + \sigma_{33})/3 \quad (4)$$

3. Results and discussion

In this study NMR and NQR parameters were calculated to show the hydrogen-bonding effects on the CS and EFG tensors at the sites of oxygen, nitrogen, carbon, and hydrogen nuclei in the chitosan/HI salt crystalline structure. To the best of our knowledge, there are no experimental NMR and NQR data for the hydrogen and oxygen nuclei; however, ^{13}C and ^{15}N NMR parameters were reported for some chitosan derivatives in the literature.[13,14] The following text will separately discuss the calculated CS and EFG tensors at the sites of various nuclei.

3.1. ^{13}C chemical shifts

Previous extensive ^{13}C NMR calculations reveal the reliability of quantum mechanical based approaches for ^{13}C chemical shielding isotropic and anisotropic calculations in the various molecular clusters.[40–43] Ramamoorthy and co-workers showed that at the DFT level, the quantum mechanical calculations have reproduced the experimental ^{13}C NMR chemical shifts in solid peptides.[44] The calculated results of ^{13}C chemical shifts with experimental data are tabulated in Table 2, and typical calibration plots are shown in Figure 2. As can be seen from Figure 2, there is a good agreement between the experimental and calculated δ_{iso} values, where a least squares fit of all data gives a strong linear relationship with an $R^2 = 0.97$. More specifically, as Table 2 indicates, the theoretical ^{13}C chemical shift results overestimate experimental values, and the B3LYP/6-311++G (d,p) data deviate by 1.4–9.8 ppm from the experimental data. It is also evident from Figure 2 that the results of the 6-311++G (d,p) basis set are more reliable than those of the 6-31++G (d,p) basis set. Furthermore, it is apparent from Table 2 that the full double-zeta basis set, 6-31++G (d,p), performs at least equally well with the B3LYP functional as the valence triple-zeta and larger basis sets that are often used.

The advantage of using the cluster model is that one can dissect different intermolecular interactions explicitly. However, due to the high computational expenses of using large clusters with large basis sets, this method generally employs only a single shell of the molecular species that directly interacts with the central molecule of interest, and even in this situation sometimes only fragments of the interacting chemical species can be

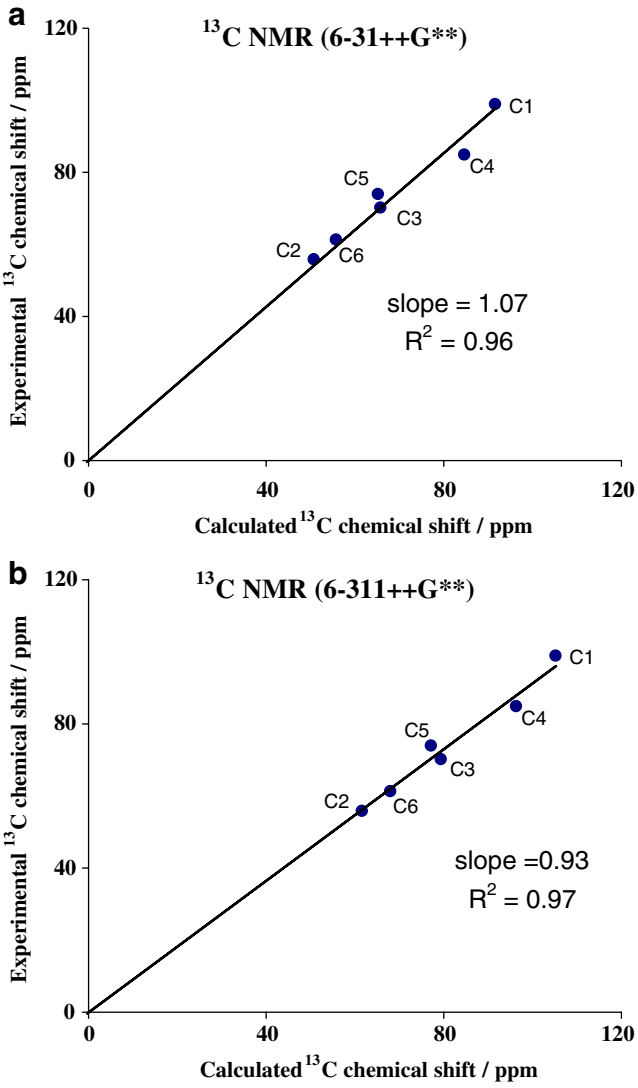

Figure 2. Plots of the experimental values versus the calculated values of the ^{13}C NMR chemical shift.

considered to restrict the method to short-range interactions. The good agreement between the calculated and experimental ^{13}C chemical shifts indicates that the HB and short-range electrostatic effects encountered in the crystalline structure are sufficiently represented by our model.

3.2. ^{17}O CS and EFG tensors

This section focuses on the calculated CS and EFG tensors at the sites of ^{17}O nuclei in the monomer and cluster models of the chitosan/HI crystalline structure (Table 3). As Figure 1 indicates, the HBs at the O-6 H site of the target molecule involve the I_3 and $-NH_3^+$ groups of the neighboring molecules. X-ray crystallography data reveal that the chitosan/HI salt makes a layer-like structure in the crystalline phase.[23] A quick look at the entire unit cell shows that an O-6···H–N type hydrogen bond joins the molecules in the two neighboring anti-parallel layers. Our earlier study on the anhydrous polymorph of chitosan suggested the significance of including this hydrogen bonding interaction in determining the ^{17}O CS and EFG tensors as well as their relative orientations.[30]

As the results in Table 3 illustrate, from the monomer to the target molecule in the cluster, the CS tensor at the site of ^{17}O-6 nucleus is significantly influenced by hydrogen-bonding interactions. More specifically, σ_{11} with 73.2 ppm reduction is the most affected principal component of the O-6 nucleus from the monomer to the central molecule in cluster. It is also interesting to see that the $\sigma_{iso}(^{17}O)$ is improved approximately 40 ppm depending on whether the chitosan molecule is in the monomer or in the hydrogen-bonding network. These effects suggest that the intermolecular hydrogen-bonding interactions at the O_6–H site of the crystalline chitosan/HI complex is rather strong. On the other hand, the calculated CS tensors of the O-1, O-3, and O-5 nuclei show some discrepancies, although not as dramatic as the one seen for O-6.

As the results in Table 3 indicate, the calculated NQR parameters also represent some trends parallel with those discussed in the CS tensors for various ^{17}O nuclei of the chitosan/HI salt. A B3LYP/6-311++G (d,p) calculation reveals that, due to the hydrogen-bonding interactions, the C_Q and η_Q parameters of the O-6 nucleus change by 2.55 MHz and 0.09 units from the isolated monomer to the target molecule in the cluster, respectively. It should be noted that these changes are much larger than those seen for our previously studied crystalline anhydrous chitosan (ca. $\Delta C_Q(^{17}O\text{-}6) = 0.24$ MHz).[30] Comparison of the structural parameters of these two compounds in their crystalline phases indicates that, unlike hydrogen bond length that contributes to the different chemical environment, there is also a difference in the hydrogen-bonding nature, O–H···O versus O–H···I, from anhydrous to the chitosan/HI salt. The $r_{O\cdots H-N}$ parameter for the anhydrous form is shown to be 1.602 Å,[30] while the corresponding value for chitosan/HI is 1.86 Å.

3.3. ^{15}N CS and ^{14}N EFG tensors

Table 4 shows the calculated NMR and NQR parameters for the nitrogen nuclei in the two models of the monomer and the cluster chitosan/HI. Similar to the previous section, both the CS and EFG tensors at the site of nitrogen are influenced by the hydrogen-bonding interactions. As can be seen from Figure 1, in the crystalline phase, the nitrogen atom interacts with the oxygen atom of the neighboring chain and two iodine ions. As Table 4 indicates, due to the hydrogen-bonding interactions, all three ^{15}N CS tensor components deviate

significantly from the monomer values. From the definition of Eq. 4 in Section 2, there is also a remarkable change in the σ_{iso} parameter from the monomer to the target molecule in the cluster (ca. 18.40 ppm). However, the calculated isotropic chemical shift value for the monomer, $\delta_{iso}(^{15}N)$, meets reasonably the available experimental data (see Table 4).[14]

As the results of Table 4 show, the calculated $C_Q(^{14}N)$ value at the $-NH_3^+$ site exhibits a rather strong dependency on the hydrogen-bonding interactions. This is consistent with the general observation that the hydrogen bonding interactions tend to reduce the $C_Q(^{14}N)$ values.[31–33] Because of the presence of the neighboring molecules, the $C_Q(^{14}N)$ parameter of the chitosan/HI complex decreases by 1.73 MHz from the isolated gas phase to the target molecule in the cluster model. These features reveal the major role of the $-NH_3^+$ group in contributing to the intermolecular hydrogen-bonding interactions in the crystalline chitosan/HI structure.

3.4. ^{1}H CS and ^{2}H EFG tensors

As discussed above, the CS and EFG tensors at the sites of the oxygen and nitrogen nuclei are significantly influenced by hydrogen-bonding interactions. The effects of HBs on the ^{1}H CS and ^{2}H EFG tensors are discussed in this section (Table 5). Hydrogen nuclei contribute to different HB types including N–H···I, N–H···O, and O–H···I (Table 1); therefore, their influence on the NMR tensors is different for various nuclei. It is noted that the changes of calculated CS and EFG tensors because of HB are parallel to each other, which shows the advantage of calculations of both terms in the study of HB interactions. The NMR and NQR parameters of those hydrogen atoms that contribute to HB interactions undergo significant changes; however, other nuclei feel less change instead.

3.5. Orientation of the EFG and CS tensors in the molecular frame of reference

High-level quantum chemical calculations have proven to be an excellent approach for obtaining CS and EFG tensor orientations in the molecular frame axes. Previously, reports in the literature have indicated that the quantum chemical calculation at the B3LYP/6-311++G (d,p) level can produce reliable results for the CS and EFG tensor orientations, although the magni-

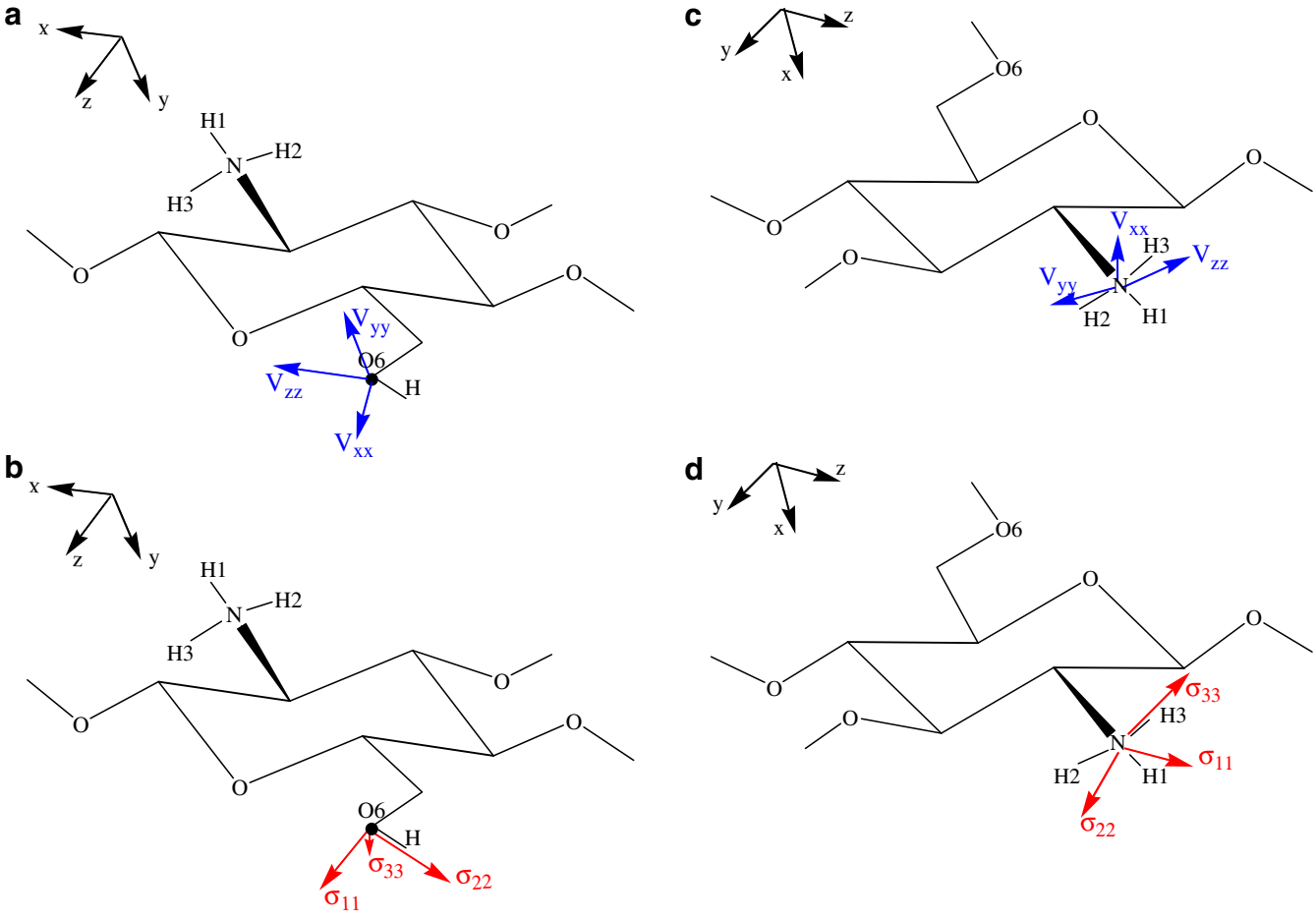

Figure 3. Relative orientation of the oxygen and nitrogen EFG and CS tensors of the chitosan salt in the molecular frame axes.

Table 6. Relative orientation of the EFG and CS tensors in the molecular frame axes[a]

Nuclei	α	β	γ
O-6	118.19	149.28	61.16
N	91.80	146.90	94.63
N–H···I-1	166.55	79.68	81.23
N–H···I-2	20.16	74.96	106.24
N–H···O-6	166.32	65.59	114.78
O-6–H···I	5.58	98.03	98.18

[a] Values in degree.

tude of the individual principal components computed by this level is less accurate.[45–48] Therefore, at this point, it is of much interest to characterize the relative orientation of the principal components of the chemical shift and EFG tensors in the molecular frame. To fulfill the objective, the calculated CS and EFG tensors of the oxygen and nitrogen atoms have been analyzed systematically to obtain their relative orientations (see Fig. 3). The calculated Euler angles (α, β, and γ) are also tabulated in Table 6.

As Figure 3 illustrates, at the O-6 nucleus, the σ_{22} is the unique component that lies approximately to the O–H bond direction where the least shielded component, σ_{11}, tends to lie in the C-6–O-6 direction. For the EFG tensor, the V_{xx} and V_{zz} components are in the plane involving the H-6–O-6–C-6 bond. More specifically, the V_{yy} component orientates approximately along the norm of this plane. Such orientations are in agreement with our previous study.[30] However, at the nitrogen site, the relative orientations of the CS and EFG tensors have different trends. As indicated in Figure 3, the V_{xx} is directed perpendicular to the amine plane where the most shielded NMR component, σ_{33} makes an approximately 90° angle with the N–C-2. This general observation was found to be essentially the same with that of our previous study on the anhydrous form of chitosan.[30] These features indicate that the presence of iodide ions remarkably changes the magnitude of the CS and EFG principal components. However, the results obtained in this paper show that neither changes in the nature of the hydrogen-bonding interactions nor the polysaccharide chain rearrangement affect on the relative orientation of the CS and EFG tensors of O-6 and the nitrogen nuclei.

4. Conclusion

In the present work, DFT calculations were performed to obtain CS and EFG tensors of nitrogen, oxygen, and hydrogen atoms. These calculations were done for both isolated gas-phase and a hydrogen-bonded cluster of chitosan. The difference between the calculated NMR and NQR parameters for those nuclei contributing in HBs shows how much these nuclei contribute in the interaction. However, for nitrogen from the monomer to the target molecule, HBs make a remarkable reduction in CS and EFG tensors. This nucleus contributes in two N–H···O and N–H···I types HBs that cause a large reduction in the quadrupole coupling constant and isotropic CS ($\Delta C_Q = 1.19$ MHz and $\Delta\sigma_{iso} = 18.39$ ppm). These results indicate that in addition of nitrogen, O-6 and H-6 are the most important nuclei of the chitosan/HI salt to confirm the crystalline structure of this compound. In addition, the CS tensors of ^{13}C were determined. The calculated CS of ^{15}N and ^{13}C are in good agreement with the experimental results. The experimental values of the ^{13}C chemical shifts were plotted versus the calculated values (Fig. 2). Good agreement of the experimental and calculated results could be seen in these plots (slope = 0.93 and $R^2 = 0.97$ for 6-311++G (d,p) basis set), too. It is determined that the B3LYP/6-311++G (d,p) data deviate by 1.4·9.8 ppm from the experimental data. This illustrates that our selected molecular cluster involves appropriately all intermolecular interactions as close as the chitosan/HI solid phase. Finally, the orientation of the CS EFG tensors at the O-6 and nitrogen sites was obtained. Our theoretical calculation indicated that at the O-6 site the σ_{22} component lies in the O-6···I hydrogen-bond direction, where for the EFG tensor, the V_{yy} component is directed perpendicular to the H–O-6–C-6–V_{zz}.

References

1. Ravi Kumar, M. N. V. *React. Funct. Polym.* **2000**, *46*, 1–27.
2. Krajewska, B. *Enzyme Microb. Technol.* **2004**, *35*, 126–139.
3. Shahidi, F.; Arachchi, J. K. V.; Jeon, Y. *Trends Food Sci. Technol.* **1999**, *10*, 37–51.
4. Vila, A.; Sanchez, A.; Janes, K.; Behrens, I.; Kissel, T.; Jato, J. L. V.; Alonso, M. J. *Eur. J. Pharm. Biopharm.* **2004**, *57*, 123–131.
5. Prashanth, K. V. H.; Tharanathan, R. N. *Biochim. Biophys. Acta Gen. Subj.* **2005**, *1722*, 22–29.
6. Krajewska, B. *Enzyme Microb. Technol.* **2004**, *35*, 126–139.
7. Senel, S.; Mc Clure, S. J. *Adv. Drug Delivery Rev.* **2004**, *56*, 1467–1480.
8. Yui, T.; Imada, K.; Okuyama, K.; Obta, Y.; Suzuki, K.; Ogawa, K. *Macromolecules* **1994**, *27*, 7601–7605.
9. Brugnerotto, J.; Desbrières, J.; Roberts, G.; Rinaudo, M. *Polymer* **2001**, *42*, 09921–09927.
10. Van de Velde, K.; Kiekens, P. *Carbohydr. Polym.* **2004**, *58*, 409–416.
11. Heux, L.; Brugnerotto, J.; Desbrières, J.; Vessali, M. F.; Rinaudo, M. *Biomacromolecules* **2000**, *1*, 746–751.
12. Duarte, M. L.; Ferreira, M. C.; Marvao, M. R.; Rocha, J. *Int. J. Biol. Macromol.* **2001**, *28*, 359–363.
13. Saito, H.; Tabeta, R.; Ogawa, K. *Macromolecules* **1987**, *20*, 2424–2430.
14. Yu, G.; Morin, F. G.; Nobes, G. A. R.; Marchessault, R. H. *Biomacromolecules* **1999**, *32*, 518–520.
15. Kameda, T.; Miyazawa, M.; Ono, H.; Yoshida, M. *Macromol. Biosci.* **2005**, *5*, 103–106.

16. Amornrat, L.; Shingo, Y.; Keiichi, N.; Ogawa, K.; Okuyama, K. *Carbohydr. Res.* **2004**, *339*, 825–833.
17. Amornrat, L.; Keiichi, N.; Ogawa, K.; Okuyama, K. *Carbohydr. Res.* **2004**, *339*, 835–843.
18. Ogawa, K.; Yui, T.; Okuyama, K. *Int. J. Biol. Macromol.* **2004**, *34*, 1–8.
19. Okuyama, K.; Noguchi, K.; Kanenari, M.; Egawa, T.; Ogawa, K. *Carbohydr. Polym.* **2000**, *41*, 237–247.
20. Kawada, J.; Yui, T.; Okuyama, K.; Ogawa, K. *Biosci. Biotechnol. Biochem.* **2001**, *65*, 2542–2547.
21. Brunner, E.; Sternberg, U. *Prog. Nucl. Magn. Reson. Spectrosc.* **1998**, *32*, 21–57.
22. Sack, I.; Machol, S. *Appl. Magn. Reson.* **1999**, *17*, 413–431.
23. Lertworasirikul, A.; Yokoyama, S.; Noguchi, K.; Ogawac, K.; Okuyama, K. *Carbohydr. Res.* **2004**, *339*, 825–833.
24. Kaupp, M.; Malkin, V. G.; Malkina, O. L.; Salahub, D. R. A. *J. Am. Chem. Soc.* **1995**, *117*, 1851–1852.
25. Nash, C. S.; Bursten, B. E. *J. Phys. Chem. A* **1999**, *103*, 632–636.
26. Lantto, P.; Vaara, J.; Kantola, A. M.; Telkki, V.; Schimmelpfenning, B.; Ruud, K.; Jokisaari, J. *J. Am. Chem. Soc.* **2002**, *124*, 2762–2771.
27. Frisch, M. J.; Trucks, G. W.; Schlegel, H. B.; Scuseria, G. E.; Robb, M. A.; Cheeseman, J. R.; Akrzewski, V. G.; Montgomery, G. A., Jr.; Stratmann, R. E.; Burant, J. C.; Dapprich, S.; Millam, J. M.; Daniels, A. D.; Kudin, K. N.; Strain, M. C.; Farkas, O.; Tomsai, J.; Barone, V.; Cossi, M.; Cammi, R.; Mennucci, B.; Pomelli, C.; Adamo, C.; Clifford, S.; Ochterski, J.; Petersson, G. A.; Ayala, P. Y.; Cui, Q.; Morokuma, K.; Malick, D. K.; Rabuck, A. D.; Raghavachari, K.; Foresman, J. B.; Cioslowski, J.; Ortiz, J. V.; Stefanov, B. B.; Liu, G.; Liashenko, A.; Piskorz, P.; Komaromi, I.; Comperts, R.; Martin, R. L.; Fox, D. J.; Keith, T.; Al-Laham, M. A.; Peng, C. Y.; Nanayakkara, A.; Gonzalez, C.; Challacombe, M.; Gill, P. M. W.; Johnson, B. G.; Chen, W.; Wong, M. W.; Andres, J. L.; Head-Gordon, M.; Replogle, E. S.; Pople, J. A. GAUSSIAN *98, Revision A.7*; Gaussian: Pittsburgh, PA, 1998.
28. Wolinski, K.; Hinton, J.; Pulay, P. *J. Am. Chem. Soc.* **1990**, *112*, 8251–8260.
29. Clark, T.; Chandrasekhar, J.; Spitznagel, G. W.; Schleyer, P. v. R. *J. Comput. Chem.* **1983**, *4*, 294–301.
30. Esrafili, M. D.; Elmi, F.; Hadipour, N. L. *J. Phys. Chem. A* **2007**, *111*, 963–970.
31. Elmi, F.; Hadipour, N. L. *J. Phys. Chem. A* **2005**, *109*, 1729–1733.
32. Mirzaei, M.; Hadipour, N. L. *J. Phys. Chem. A* **2006**, *110*, 4833–4838.
33. Behzadi, H.; Hadipour, N. L.; Mirzaei, M. *Biophys. Chem.* **2007**, *125*, 179–183.
34. Chen, X.; Zhan, C. *THEOCHEM* **2004**, *682*, 73–82.
35. Ida, R.; Clerk, M.; Wu, G. *J. Phys. Chem. A* **2006**, *110*, 1065–1071.
36. Pyykkö, P. *Mol. Phys.* **2001**, *99*, 1617–1629.
37. Wasylishen, R. E.; Mooibroek, S.; Macdonald, J. B. *J. Chem. Phys.* **1984**, *81*, 1057–1059.
38. Anderson-Altmann, K. L.; Phung, C. G.; Mavromoustakos, S.; Zheng, Z.; Facelli, J. C.; Poulter, C. D.; Grant, D. M. *J. Phys. Chem.* **1995**, *99*, 10454–10458.
39. Jameson, A. K.; Jameson, C. *Chem. Phys. Lett.* **1987**, *134*, 461–466.
40. Lumsden, M. D.; Wasylishen, R. E.; Eichele, K.; Schindler, M.; Penner, G. H.; Power, W. P.; Curtis, R. D. *J. Am. Chem. Soc.* **1994**, *116*, 1403–1413.
41. Sun, H.; Sanders, L. K.; Oldfield, E. *J. Am. Chem. Soc.* **2002**, *124*, 5486–5495.
42. Hoshiba, T.; Ida, T.; Mizuno, M.; Otsuka, T.; Takaoka, K.; Endo, K. *J. Mol. Struct.* **2002**, *602–603*, 381–388.
43. Nakatsuji, H.; Kanda, K.; Endo, K.; Yonezawa, T. *J. Am. Chem. Soc.* **1984**, *106*, 4653–4660.
44. Birn, J.; Poon, A.; Mao, Y.; Ramamoorthy, A. *J. Am. Chem. Soc.* **2004**, *126*, 8529–8534.
45. Wu, G.; Dong, S.; Ida, R.; Reen, N. *J. Am. Chem. Soc.* **2002**, *124*, 1768–1777.
46. Wong, A.; Kevin, K. J.; Jenkins, R.; Clarkson, G. J.; Anupõld, T.; Howes, A. P.; Crout, D. H. G.; Samoson, A.; Dupree, R.; Smith, M. E. *J. Phys. Chem. A* **2006**, *110*, 1824–1835.
47. Bulter, G.; Brown, T. L. *J. Am. Chem. Soc.* **1981**, *103*, 6541–6549.
48. Gready, J. E. *J. Phys. Chem.* **1984**, *88*, 3497–3503.